Mechanistic Studies of *Bacillus subtilis* QueF, the Nitrile Oxidoreductase Involved in Queuosine Biosynthesis[†]

Bobby W. K. Lee, Steven G. Van Lanen, and Dirk Iwata-Reuyl*

Department of Chemistry, Portland State University, P.O. Box 751, Portland, Oregon 97201-0751

Received June 28, 2007; Revised Manuscript Received August 22, 2007

ABSTRACT: The enzyme QueF was recently identified as an enzyme involved in the biosynthesis of queuosine, a 7-deazaguanosine modified nucleoside found in bacterial and eukaryotic tRNA. QueF exhibits sequence homology to the type I GTP cyclohydrolases characterized by FolE, but contrary to the predictions based on sequence analysis the enzyme in fact catalyzes a mechanistically unrelated reaction, the NADPH-dependent reduction of 7-cyano-7-deazaguanine ($preQ_0$) to 7-aminomethyl-7-deazaguanine ($preQ_1$), a late step in the queuosine pathway. The reduction of a nitrile is unprecedented in biology, and we report here characterization and mechanistic studies of the enzyme from *Bacillus subtilis*. The recombinant enzyme exhibits optimal activity at pH 7.5 and moderate ionic strength, and is not dependent on metal ions for catalytic activity. Steady-state kinetic analysis provided a $k_{cat} = 0.66 \pm 0.04$ min^{-1}, K_M ($preQ_0$) $= 0.237 \pm 0.045$ μM, and K_M (NADPH) $= 19.2 \pm 1.1$ μM. Based on sequence analysis and homology modeling we predicted previously that Cys^{55} would be present in the active site and in proximity to the nitrile group of $preQ_0$. Consistent with that prediction we observed that the enzyme was inactivated when preincubated with iodoacetamide, and protected from inactivation when $preQ_0$ was present. Furthermore, titrations of the enzyme with $preQ_0$ in the absence of NADPH were accompanied by the appearance of a new absorption band at 376 nm in the UV−vis spectrum consistent with the formation of an α,β-unsaturated thioimide. Site-directed mutagenesis of Cys^{55} to Ala or Ser resulted in loss of catalytic activity and no absorption at 376 nm upon addition of $preQ_0$. Based on our data we propose a chemical mechanism for the enzyme-catalyzed reaction, and a chemical rationale for the observation of covalent catalysis.

We recently reported the discovery of a new protein family involved in nitrile metabolism, QueF, which catalyzes the NADPH-dependent reduction of the nitrile group to a primary amine (*1*), the first example of the biological conversion of a nitrile containing metabolite to the corresponding amine. The QueF activity is observed in the biosynthesis of the tRNA-modified nucleoside queuosine (Q[1]), where it catalyzes the 2-fold reduction of the advanced intermediate $preQ_0$ (7-cyano-7-deazaguanine) to $preQ_1$ (7-aminomethyl-7-deazaguanine) (Figure 1). $PreQ_1$ is subsequently inserted into the tRNA by the enzyme TGT (*2*), and the remainder of the pathway occurs at the level of the tRNA (*3*).

The discovery of QueF activity expands the chemistry of known nitrile metabolizing enzymes (*4*), which includes hydrolysis (nitrile hydratase and nitrilase), oxidation (oxygenase), and cleavage (hydroxynitrile lyase). The discovery of QueF also adds to a small group of enzymes traditionally classified as $NAD(P)^+$-dependent four-electron-transfer dehydrogenases (*5*). These include UDP-glucose dehydrogenase (and its homologues UDP-*N*-acetylmannosamine dehydrogenase and GDP-mannose dehydrogenase), histidinol dehydrogenase, and 3-hydroxy-3-methylglutaryl-coenzyme A (HMG-CoA) reductase, all of which have enzymatic activities equivalent to both an alcohol and aldehyde dehydrogenase.

Despite the similarities in the overall chemistry catalyzed by the dehydrogenase enzymes above, they lack significant sequence homology and have been found to employ distinctly different chemical mechanisms. In the case of UDPGlcDH, an active site cysteine has been implicated in covalent catalysis (*6*, *7*) in the mechanistic regime of the aldehyde-oxidizing enzymes, for which glyceraldehyde-3-phosphate dehydrogenase (GAPDH) is the archetype. Histidinol dehydrogenase, although containing two strictly conserved cysteine residues, is a Zn^{2+}-dependent metalloenzyme, and biochemical and structural data suggests that the reaction mechanism is facilitated only by acid−base catalysis (*8*). HMG-CoA reductase does not employ covalent catalysis nor is it metal-dependent (*9*, *10*), although the action on the thioester substrate may be thought to resemble the GAPDH archetype in its chemistry of aldehyde oxidation. Similarly, while nitrile hydratases (NHases) and nitrilases both catalyze hydrolysis reactions (to amides and carboxylic acids, respectively), their catalytic mechanisms are quite distinct.

[†] We thank the NSF (MCB9733746) and NIH (GM070641-01A3) for their generous financial support of this work.

* To whom correspondence should be addressed. E-mail: iwatareuyld@pdx.edu. Tel: 503-725-5737. Fax: 503-725-9525.

[1] Abbreviations: tRNA, transfer ribonucleic acid; Q, queuosine; $preQ_0$, 7-cyano-7-deazaguanine; $preQ_1$, 7-aminomethyl-7-deazaguanine; NADPH, reduced β-nicotinamide adenine dinucleotide phosphate; $NADP^+$, oxidized β-nicotinamide adenine dinucleotide phosphate; TGT, tRNA-guanine transglycosylase; DTT, dithiothreitol; SDS−PAGE, sodium dodecyl sulfate polyacrylamide gel electrophoresis; HPLC, high pressure liquid chromatography; DMSO, dimethyl sulfoxide; PCR, polymerase chain reaction; HEPES, (*N*-[2-hydroxyethyl]piperazine-*N*[1]-[2-ethanesulfonic acid]); Tris, tris(hydroxymethyl)aminomethane; ACES, *N*-(2-acetamido)-2-aminoethanesulfonic acid.

10.1021/bi701265r CCC: $37.00 © 2007 American Chemical Society
Published on Web 10/11/2007

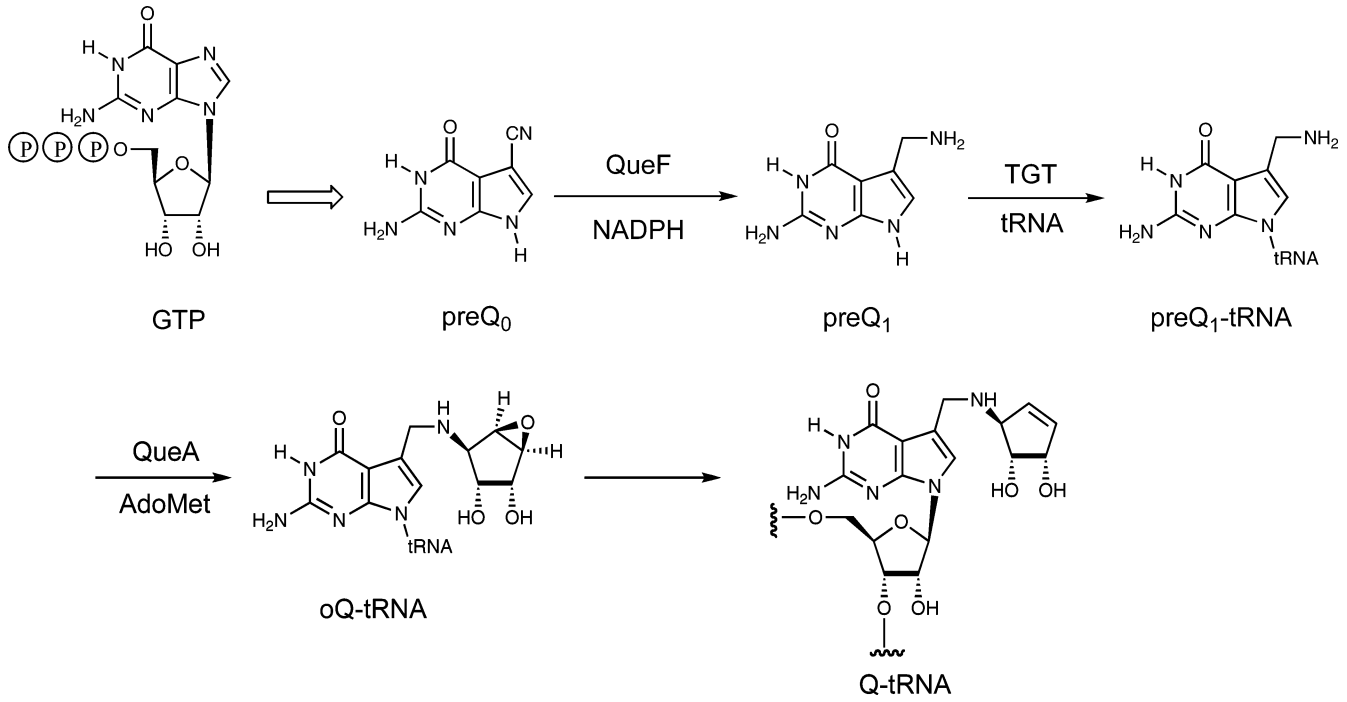

FIGURE 1: Biosynthetic pathway to queuosine in bacteria.

NHases are metal-dependent enzymes, requiring either Co^{3+}, Fe^{2+}, or Zn^{2+} to co-ordinate an active site water molecule (*11*−*13*), while nitrilases utilize a conserved cysteine residue as a catalytic nucleophile (*14*, *15*), forming a covalent thioimide intermediate in the reaction. This latter mode of reactivity is also observed in a papain mutant engineered to catalyze nitrile hydrolysis (*16*, *17*).

Structural and sequence analysis indicate that the QueF enzymes belong to the tunnel-fold (T-fold) superfamily (*1*), a structural superfamily of functionally distant proteins that bind planar pterin/purine substrates (*18*). The fundamental building block of T-fold proteins is a small monomeric unit composed of a pair of 2-stranded antiparallel β-sheets and 2 antiparallel α-helices. These assemble into homo oligomers that form a $\beta_{2n}\alpha_n$ barrel, with 2 barrels joining in a head-to-head orientation to form the active enzyme (*18*). The active sites of T-fold proteins all occur at the interface of subunits, with residues from separate monomers contributing to the active-site architecture. Among the conserved sequence elements of QueF family members is an invariant cysteine residue (Cys^{55} in the *Bacillus subtilis* orthologue) that is also conserved in GTP cyclohydrolase I (FolE), another T-fold member that exhibits the highest homology to QueF (*1*). In FolE this cysteine residue is located in the active site where it serves as a ligand to an essential Zn^{2+} atom (*19*). The Zn^{2+} in turn binds and activates a water molecule for nucleophilic attack at C-8 of GTP in the first catalytic step of the reaction. A homology model of QueF with the substrate $preQ_0$ docked in the putative active site indicated that, like FolE, Cys^{55} was located in the active site and in close proximity to the nitrile, and thus might play an important role in catalysis (*20*).

In this report we present the results of our biochemical characterization of *B. subtilis* QueF, a prototypic member of the QueF family of enzymes, as well as experiments designed to elucidate the catalytic mechanism of biological nitrile reduction, in particular, the role of Cys^{55} in this process.

MATERIALS AND METHODS

General. Buffers and salts of highest quality grade were purchased from Sigma unless otherwise noted. DTT was from U.S. Biologicals. Iodoacetamide was from Amersham Biosciences. Plasmid Mini-Kits were from Qiagen. Dialysis was performed in Slide-A-Lyzer cassettes from Pierce. Oligonucleotides were from Integrated DNA Technologies, Inc. β-NADPH and β-$NADP^+$ were from Research Products International Corp. Protein concentrations were based on the Bradford dye-binding procedure (*21*) and by direct UV measurement (ϵ_{280} = 23,660 M^{-1}) following the procedure described by von Hippel (*22*). Recombinant *B. subtillis* QueF was purified as described previously (*1*) and provided protein that was homogeneous by SDS−PAGE. The substrate $preQ_0$ was synthesized as described (*23*) and purified by reverse phase HPLC. Stock solutions of $preQ_0$ were prepared in DMSO using ϵ_{262} = 10,453 M^{-1} (*23*). Data analysis and graphing were carried out using the Kaleidagraph software package (Synergy Software, Reading, PA).

Instrumentation. PCR was carried out on a GeneAmp PCR system 2400 from Perkin-Elmer Life Sciences. An Amersham Biosciences Typhoon 9200 variable mode imager with ImageQuant 5.2 software was used for fluorescence detection of ethidium bromide stained agarose gels. UV−vis spectroscopy was performed with a Varian Cary 100 Bio equipped with a thermostated cell holder. Fluorescence spectroscopy was carried out on a QM3 spectrofluorimeter from Photon Technology International. HPLC was carried out using a Hitachi L-7100 pump system with an L-4500A photodiode array detector, and controlled via the Hitachi ConcertChrome software. Circular dichroism spectroscopy was performed with an Aviv 202 recording spectropolarimeter equipped with a Peltier thermostated cell holder and using a 1.0 mm path length rectangular cell. Protein mass

spectrometry was carried out at the Proteomics Shared Resource facility at Oregon Health & Science University, Portland, OR, using a QSTAR XL quadrupole time-of-flight mass spectrometer (Applied Biosystems/MDS Sciex, Foster City, CA) equipped with a standard ion source (MDS Sciex, Concord, Canada). DNA sequencing was performed at the PSU-Keck Genomics facility.

pH Profile and Ionic Strength. Optimal pH for enzymatic activity was determined using a 3 buffer system of Tris−ACES−ethanolamine (100−50−50 mM) as described (*24*). The pH profile for QueF was carried out at 30 °C in 50 mM buffer, 100 mM KCl, 100 μM $preQ_0$, 100 μM NADPH, and 0.5 μM QueF. Optimal ionic strength conditions were tested in 100 mM HEPES (pH 7.5), 100 μM $preQ_0$, 100 μM NADPH, and 1 μM QueF at 30 °C.

Metal Analysis. The activity of QueF was assessed with the chloride salts of Ca^{2+}, Mg^{2+}, Mn^{2+}, Co^{2+}, Ni^{2+}, Zn^{2+}, Fe^{2+}, and Fe^{3+}; Cu^{2+} was investigated as the sulfate salt. Ferrous iron was prepared in sodium acetate (pH 5.4) with ascorbic acid as described (*25*). Reactions contained 50 mM HEPES (pH 7.25), 100 mM NaCl, 100 μM $preQ_0$, 100 μM NADPH, 100 μM metal (or EDTA), and 1.0 μM QueF. Assays were run at 30 °C for 5 min and 1 h.

Steady-State Kinetic Analysis. NADPH and $NADP^+$ concentrations were determined at pH 7.0 using $\epsilon_{340} = 6220$ M^{-1} and $\epsilon_{260} = 18{,}000$ M^{-1}, respectively. For the determination of the NADPH kinetic parameters the reaction assays contained 100 mM Tris (pH 7.5), 100 mM KCl, 1 mM DTT, 20 μM $preQ_0$, 0.776 μM QueF, and variable NADPH (5−140 μM). The reaction assays were monitored by following the oxidation of NADPH at 340 nm for 120 s at 30 °C. For the determination of the $preQ_0$ kinetic parameters the progress of the reaction was monitored by fluorescence detection of the alkaline $NADP^+$ product as previously described (*26*). The assays contained 100 mM phosphate buffer (pH 7.5), 100 mM KCl, 1 mM DTT, 400 μM NADPH, 0.025 μM QueF, and variable $preQ_0$ (0.066−2.0 μM) at 30 °C. The reaction assays were initiated by the addition of enzyme unless otherwise noted. At the time specified, aliquots of 50 μL were transferred to an equivalent volume of 0.3 M HCl and incubated for 10 min at room temperature. Fifty microliters of the HCl-treated sample was then removed and added to 200 μL of 9.0 M NaOH, mixed thoroughly, and placed in the dark. The product was left to develop in the dark for 2.5 h before analysis. Prior to analysis, 100 μL of the resulting alkaline solution was added to 2.5 mL of water for measurement. Fluorescence was measured with an excitation wavelength of 360 nm and an emission wavelength of 455 nm. The excitation and emission slit widths were set to 10 nm. A control assay was performed in the absence of $preQ_0$, and product concentrations were determined from a standard curve of $NADP^+$ prepared analogously to the reaction assays. Initial velocity data were fit to the equations describing a bi−uni−uni−bi ping-pong ter ter kinetic mechanism, with $preQ_0$ as the leading substrate (eq 1) and both NADPH molecules binding with equal affinity (eq 2). The data represent the average of at least 3 independent runs, each carried out in duplicate, with the uncertainty in the values of the kinetic constants expressed as the standard error.

$$v = \frac{V_{max}[A]}{K_{M_A}\left(1 + \frac{K_{i_A}K_{M_B}}{K_{M_A}[B]}\right) + [A]\left(1 + \frac{2K_{M_B}}{[B]}\right)} \quad (1)$$

$$v = \frac{V_{max}[B]}{K_{M_B}\left(2 + \frac{K_{i_A}}{[A]}\right) + [B]\left(1 + \frac{K_{M_A}}{[A]}\right)} \quad (2)$$

Inactivation and Protection Studies of QueF. Inactivation of QueF with iodoacetamide was monitored following the oxidation of NADPH at 340 nm. Inactivation of the enzyme was measured in the absence of dithiothreitol to prevent the reaction of the inhibitor with added thiols. The inactivation was carried out as follows: enzyme (to a final concentration of 5 μM) was added to a solution of 100 mM Tris (pH 7.5), 100 mM KCl, and 50 μM iodoacetamide. At specific times, aliquots (10 μL) were removed and diluted into a standard assay solution containing 100 mM Tris (pH 7.5), 100 mM KCl, 100 μM $preQ_0$, and 100 μM NADPH, and the reaction monitored by UV−vis spectroscopy. Enzyme protection assays were performed following this method except the inactivation mixture also contained 100 μM $preQ_0$.

Preparation of Cys^{55} Mutants. Mutagenesis was carried out with the QuikChange kit (Stratagene). The sequences of the primers used for the construction of the mutant plasmids are as follows, with the mutant codon underlined.

C55A (sense):

5′-CCGGAATTCACATCTTTAGCTCCT-
AAAACAGGC-3′

C55A (antisense):

5′-CTGGCCTGTTTTAGGAGCTAAAGATGT-
GAATTCCGG-3′

C55S (sense):

5′-CCGGAATTCACATCTTTATCTCCT-
AAAACAGGC-3′

C55S (antisense):

5′-CTGGCCTGTTTTAGGAGATAAAGATGTG-
AATTCCGG-3′

The *B. subtilis* queF gene (originally denoted *ykvM*) in the pET-30Xa vector (*1*) was used as the template for the PCR to generate the single mutants. The PCR protocol consisted of an initial hold at 94 °C for 45 s, followed by 18 cycles of 94 °C for 45 s, 55 °C for 60 s, and 68 °C for 8 min. After 18 cycles, the reaction mixtures were kept at 4 °C. Dpn1 (1 μL) was added and the reaction mixture was incubated at 37 °C for 1 h before the plasmid was transformed into competent *Escherichia coli* DH5α cells. The plasmid DNA was purified using the Qiagen miniprep kit, and the mutated genes were sequenced to verify the mutation and the otherwise unaltered DNA sequence. The expression and purification of the C55A and C55S proteins were carried out as described for the wild-type protein (*1*).

Substrate Titration Studies. Titrations of QueF with $preQ_0$ were monitored in the absence of NADPH. $PreQ_0$ (3.0 mM or 500 μM in DMSO) was titrated into a solution of wild-type QueF (20 μM) or the C55S/C55A mutants (50 μM)

containing 100 mM Tris (pH 7.5), 100 mM KCl, and 1 mM DTT while monitoring the absorbance from 230 to 450 nm. The titration was continued until there was no further increase in absorbance or the ratio of substrate to enzyme reached 4. The concentration of DMSO did not exceed 5% of the total volume.

To determine the extinction coefficient of the putative thioimide adduct we constructed a standard curve of absorbance at 376 nm versus adduct concentration. Dilutions of a reaction mixture containing 10 mM phosphate (pH 7.5), 10 mM KCl, 1 mM DTT, 100 μM $preQ_0$, and 50 μM QueF were made with a buffer of 10 mM phosphate (pH 7.5), 10 mM KCl, and 1 mM DTT. A 2-fold excess of $preQ_0$ was used to ensure saturation of the protein active sites. The final protein concentrations were 0, 6.25, 12.5, 25, 37.5, and 50 μM. The resulting solutions were scanned between 230 and 450 nm, and the absorbance values at 376 nm were plotted against QueF concentrations. The data from triplicate determinations indicate that the extinction coefficient of the band at 376 nm is $4400 \pm 90\ M^{-1}$.

To assess the stability of the putative thioimide intermediate a solution of $preQ_0$ (50 μM) was added to a solution of 10 mM phosphate buffer (pH7.5), 10 mm KCl, 1 mM DTT, and 20 μM QueF, and after incubating for 5 min at room temperature and recording the UV−vis spectrum, the mixture (2 mL) was placed into a 10,000 Da molecular weight cutoff dialysis cassette and dialyzed against substrate-free buffer (4 L). After 3 h, the dialyzed material was removed, the total volume recorded (2.2 mL), a portion subjected to Bradford analysis ([QueF] = 18 μM), and another rescanned by UV−vis. To the latter sample was added NADPH (final concentration 100 μM), and the reaction was monitored at 340 nm. To another sample of the dialyzed $preQ_0$-QueF adduct was added 25 μM NADPH, and the reaction was monitored at 340 nm for 120 min and then rescanned by UV−vis.

Circular Dichroism Spectroscopy. Prior to analysis, wild-type QueF and the C55S and C55A mutants were dialyzed into 20 mM phosphate buffer (pH 7.5) and 20 mM NaF. The CD spectra were obtained at a protein concentration of 2 mg/mL in the far-UV region (180−260 nm; wavelength step 0.10 nm; averaging time 5 s) at 25 °C under a nitrogen atmosphere. Two scans were completed consecutively and the signals averaged.

Size-Exclusion Chromatography. Size-exclusion chromatography was performed on the wild-type QueF and the C55S and C55A mutants using a BioSep-SEC-S 4000 column (Phenomenex) with a mobile phase of 50 mM phosphate (pH 7.2) at 1 mL/min. The void volume (V_0) and the total bead volume (V_T) were measured with Blue Dextran (2000 kDa) and DNP-aspartate (300 Da), respectively. Calibration of the column was conducted with the following protein standards: thyroglobulin (670 kDa), apoferritin (443 kDa), pyruvate kinase (237 kDa), alcohol dehydrogenase (150 kDa), bovine serum albumin (66 kDa), and ovalbumin (44 kDa). K_D values were calculated according to the equation $K_D = (V_e - V_O)/(V_T - V_O)$, where V_e is the elution volume of the protein of interest, and then plotted versus log MW to generate the standard curve.

Protein Mass Spectrometry. Wild-type or mutant QueF proteins were first dialyzed into 5 mM Tris (pH 7.5), 5 mM KCl, and 1 mM DTT. Following concentration of the proteins to 2 mg/mL, the enzyme was portioned into 50 μL aliquots, flash frozen in liquid nitrogen, and stored at −80 °C. Prior to analysis, samples of thawed protein were mixed with an equal volume of 0.5% formic acid and injected onto the mass spectrometer. For experiments with $preQ_0$, samples of protein and $preQ_0$ were mixed and incubated at room temperature for 5 min before acidification. The concentrated samples were diluted to approximately 1 pmol/μL with 50% methanol/0.1% formic acid and then directly infused into the ion source using a 500 μL syringe at a flow rate of 5 μL/min. The instrument was externally calibrated in the positive ion mode using two fragment ion peaks (*m*/*z* 175.1190 and *m*/*z* 1285.5444) from the tandem mass spectrum of Glu-fibrinopeptide (Sigma). The following parameter settings were used to acquire mass spectra from *m*/*z* 900 to 1600 in the positive ion TOF/MS mode: spray voltage, 5500 V; curtain gas, 20; GS1 gas, 15; declustering potential (DP), 85 V; declustering potential 2 (DP2), 15 V; focusing potential (FP), 265 V; accumulation time, 1 s. Spectra were summed over a minimum of 120 scans, and the series of multiply charged ion peaks were deconvoluted by the Bayesian protein reconstruct tool (Bioanalyst QS 1.1 software package) to determine the zero charge masses of the intact proteins.

Table 1: Effect of Metal Ions on the Activity of QueF

metal ion (100 μM)	relative activity (%)
none	100
EDTA	100
Mn^{2+}	96
Mg^{2+}	74
Ca^{2+}	105
Zn^{2+}	90
Co^{2+}	95
Cu^{2+}	9
Fe^{2+}	75
Fe^{3+}	8
Ni^{2+}	104

RESULTS

pH and Salt Studies. The pH dependence of enzymatic activity under nominal V_{max} conditions was investigated over a pH range from 5.4 to 9.4 in a tribuffer system to maintain a constant ionic strength (*24*). The pH profile exhibits a rough bell curve with maximal activity at pH 7.50 (Figure S1, Supporting Information). The effect of ionic strength on enzymatic activity was investigated separately by measuring enzyme activity at pH 7.5 over a range of 500 nM to 500 mM KCl (Figure S2, Supporting Information). The enzyme was neither stimulated nor inhibited at KCl concentrations <10 mM, but showed marked inhibition when the concentration of KCl was above 100 mM.

Metal Ion Dependence. Enzyme activity was measured in the presence of a variety of divalent metals, as well as in the presence of EDTA (Table 1). Maximal enzyme activity was observed in the absence of added metal or in the presence of EDTA, indicating that the enzyme is not metal dependent. With the exception of Cu^{2+} and Fe^{3+}, most metals displayed little effect on enzyme activity (activation or inhibition) at the single concentration investigated. In contrast, Cu^{2+} and Fe^{3+} strongly inhibited enzyme activity, an effect that appeared to be irreversible.

Steady-State Kinetic Analysis. The full QueF reaction involves the binding and reaction of one molecule of $preQ_0$

and two molecules of NADPH. For initial velocity analysis of the reaction we assumed a bi−uni−uni−bi ping-pong ter ter kinetic mechanism as has been shown for other NAD(P)$^+$-dependent four-electron-transfer dehydrogenases (*6*, *27*−*29*), with $preQ_0$ binding first and both equivalents of NADPH exhibiting equal binding affinity (eqs 1 and 2). The assumption of a defined kinetic mechanism in the evaluation of initial velocity data is only of relevance for the second substrate, as all multisubstrate equations reduce to the simple Michaelis−Menten equation for the leading substrate in the presence of saturating cosubstrate. While other experiments (*vide infra*) were consistent with $preQ_0$ binding first, there is no reason *a priori* to assume that NADPH should exhibit identical K_M's for binding the two enzyme forms. Nevertheless, in the absence of specific evidence to the contrary, assuming equal affinity for both NADPH molecules satisfies the constraint of parsimony. Given the assumed kinetic mechanism, the calculated K_M for NADPH is half the value (eq 2) obtained when the standard form of the Michaelis−Menten equation is used. Thus, initial velocity analysis as a function of variable [$preQ_0$] (Figure 2A) using the fluorescent alkaline NADP$^+$ assay provided a $K_M = 0.237 \pm 0.045$ μM and $k_{cat} = 0.66 \pm 0.04$ min^{-1} (comparable to the kinetic parameters for other enzymes in the pathway (*30*, *31*)), while initial velocity analysis with variable [NADPH] (Figure 2B) using the continuous UV−vis assay provided a $k_{cat} = 0.69 \pm 0.02$ min^{-1} and a $K_M = 19.2 \pm 1.07$ μM, the latter roughly half the value we previously reported (*1*) from a preliminary kinetic analysis using the standard Michaelis−Menten equation.

Inactivation and Protection Studies. To assess the importance of Cys^{55} to the catalytic activity of QueF, we investigated the ability of iodoacetamide to inactivate the enzyme. When preincubated with iodoacetamide in 10-fold molar excess, QueF showed a time-dependent loss of enzyme activity (Figure 3A), and the enzyme was rendered essentially inactive within 8 min of preincubation. When $preQ_0$ was included at saturating concentration in the preincubation mixture, attenuation of protein inactivation was observed (Figure 3B). Under these conditions significant enzyme activity was observed even after 20 min of preincubation with iodoacetamide/$preQ_0$. The results are consistent with the hypothesis that a catalytically important Cys residue, presumably Cys^{55}, is present in the active site where it can react with iodoacetamide, and the presence of the substrate protects this residue from reaction with iodoacetamide.

Substrate Titration Studies. To further probe the binding of $preQ_0$ to the protein, titrations of substrate into enzyme were monitored by UV−vis spectroscopy. While $preQ_0$ and QueF do not show any significant absorbance beyond 320 nm (Figure 4), titrations of enzyme with $preQ_0$ result in the formation of a new peak at 376 nm (Figure 4). The rate of appearance of this absorbance is very fast, forming in the mixing time of the experiment. A plot of the absorbance values at 376 nm versus the concentration of $preQ_0$ (Figure 4, inset) shows that the absorbance plateaus when $preQ_0$ is stoichiometric with enzyme. The extinction coefficient for this new band was determined to be 4400 ± 90 M^{-1} (Figure S3, Supporting Information).

When the enzyme was incubated with excess $preQ_0$ followed by dialysis against substrate-free buffer (2000×) for 3 h, UV−vis measurements demonstrated that the 376 nm absorption band was still present (Figure 5A, inset). Based on the absorbance at 376 nm the concentration of the enzyme−$preQ_0$ adduct was calculated to be 16 μM; thus, ~89% of the protein existed as the $preQ_0$ adduct ([QueF] = 18 μM postdialysis). When excess NADPH was added to this solution and the absorbance of the cofactor monitored at 340 nm, we observed a rapid decrease in absorption, corresponding to the consumption of ~28 μM NADPH (Figure 5B) and consistent with the 2:1 stoichiometry (NADPH:$preQ_0$) of the reaction. Furthermore, in a separate experiment a stoichiometric amount of NADPH was added to a dialyzed $preQ_0$−QueF adduct, and after observing the consumption of NADPH by monitoring the cofactor absorbance at 340 nm (Figure 5C) we were able to observe, without interference by excess unreacted NADPH, that consumption of NADPH was accompanied by loss of the 376 nm absorption band (Figure 5C, inset bottom trace). With the addition of $preQ_0$ to this sample we observed the regeneration of the 376 nm absorption band (Figure 5C, inset top trace).

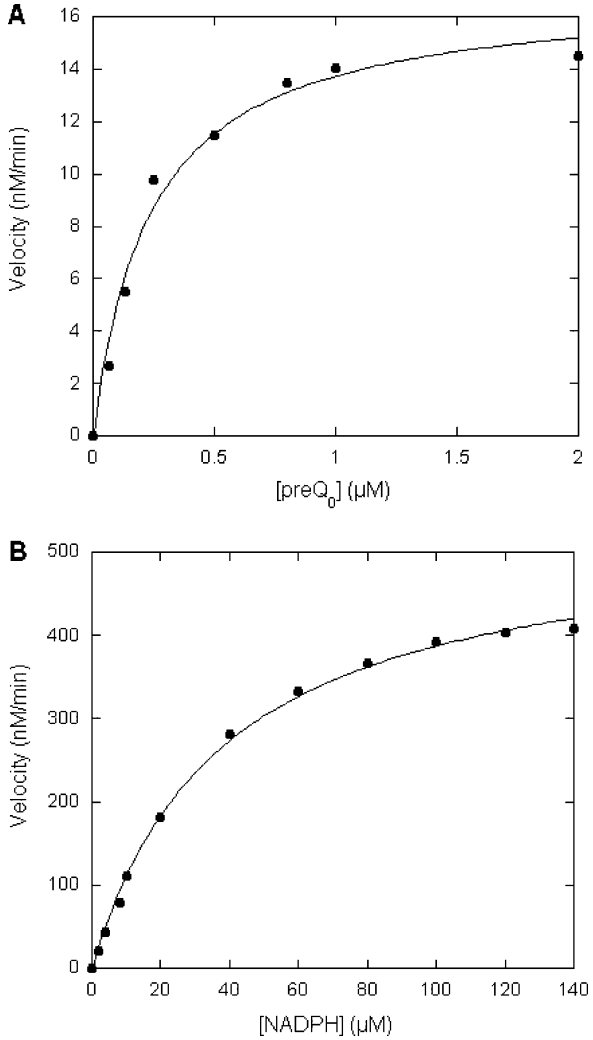

FIGURE 2: Steady-state kinetic analysis. A. For the determination of the $preQ_0$ kinetic parameters, assays were carried out in 100 mM phosphate buffer (pH 7.5), 100 mM KCl, 1 mM DTT, 400 μM NADPH, 0.025 μM QueF, with variable [$preQ_0$] from 0.66 to 2 μM. B. For the determination of the NADPH kinetic parameters, assays were carried out in 100 mM Tris (pH 7.5), 100 mM KCl, 1 mM DTT, 20 μM $preQ_0$, 0.77 μM QueF, with variable [NADPH] from 5 to 140 μM. The data points represent the averages of three replicate measurements, each carried out in duplicate.

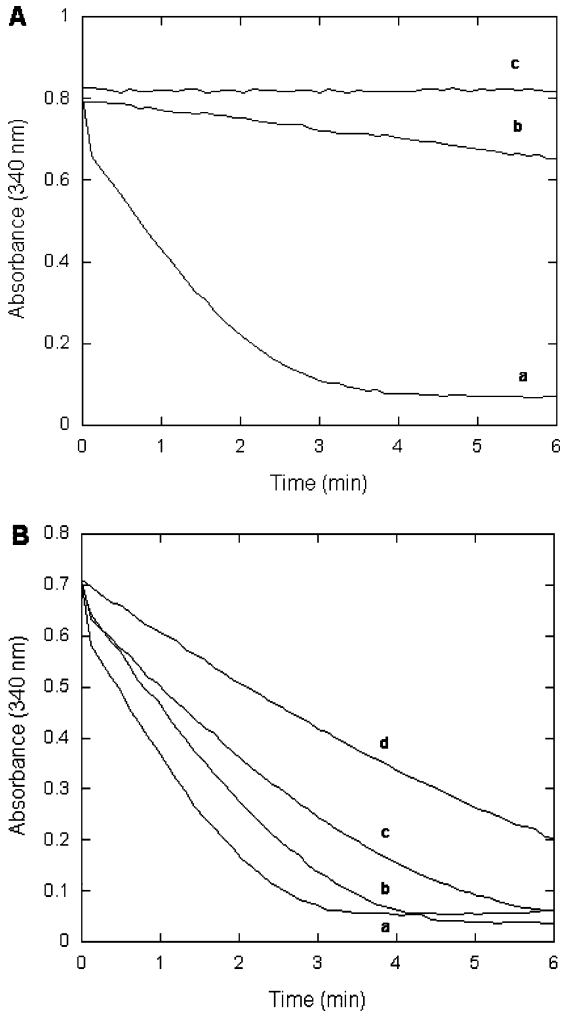

FIGURE 3: The inactivation of QueF with iodoacetamide (A) and protection of the enzyme (B) in the presence the $preQ_0$. Aliquots of a solution containing enzyme (5 μM) and iodoacetamide (50 μM) were removed at specified time points 0 min (a), 2 min (b), 8 min (c), and diluted 20-fold into to a standard assay solution containing 100 μM $preQ_0$ and 100 μM NADPH prior to analysis. The protection assays, 0 min (a), 8 min (b), 14 min (c), and 20 min (d), were carried out in the same manner except the preincubation mixture included 100 μM $preQ_0$. The assays were carried out in triplicate, and the plot shows a representative trace for assay.

Mass Spectrometry of QueF−preQ$_0$ Adducts. To investigate the presence of a covalent substrate enzyme adduct incubations of QueF with variable $preQ_0$ (1:1 to 1:5 stoichiometry) were subjected to ESI-MS. The parent molecular ion in all cases corresponded to a single subunit of the free enzyme (data not shown). Small signals due to multimers (dimer, trimer, tetramer, and pentamer) were observed, but these also corresponded to the unbound protein.

C55S, C55A Mutant Preparation and Activity Assays. The Cys^{55} point mutations were generated in the *B. subtilis* queF gene in the pET-30Xa vector using the QuikChange kit. The mutant recombinant proteins were overproduced as His_6-fusion proteins, and purification by affinity chromatography afforded pure proteins as judged by SDS−PAGE. Analysis of the recombinant proteins by ESI-MS provided parent molecular ions of 24,342 Da (C55S; $M + H^+$) and 24,327 Da (C55A; $M + H^+$), both consistent with the values of His_6-QueF (MW 24,358 Da) containing only the desired mutation (note that the N-terminal fusion containing the His_6-tag from the pET30 construct contributes 4985 Da to the molecular weight of the fusion protein). Prior to activity assays, the His_6 leader sequence was removed by Factor Xa proteolysis to provide the native N-terminii.

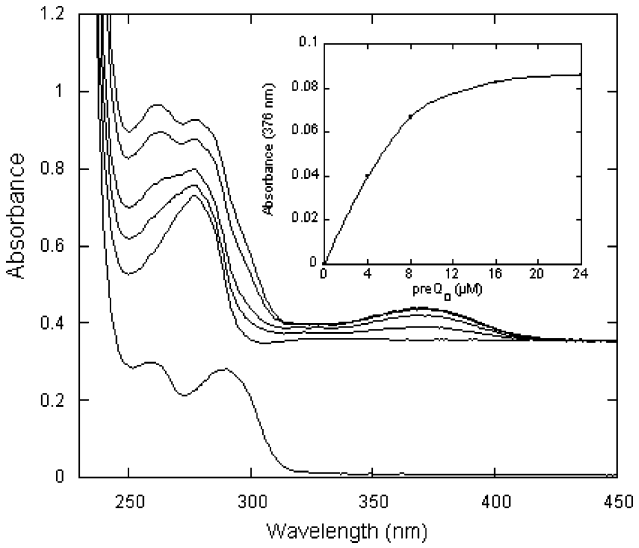

FIGURE 4: Titration of wild-type QueF with $preQ_0$. (Main plot) The lower curve displays the UV−vis spectrum of 20 mM $preQ_0$. Above, a scan of wild-type QueF alone (20 mM), followed by successive additions of $preQ_0$ to give concentrations of 4 μM, 8 μM, 16 μM, and 24 μM. (Inset) A plot of the Abs376 as a function of [$preQ_0$].

Both the C55S and C55A mutants exhibited little or no activity (<0.001% wild-type activity) when assayed by either the UV−vis (Figure 6) or fluorescent assays (Figure S4, Supporting Information), even under conditions of high substrate and enzyme concentrations. Titrations of the proteins with $preQ_0$ in the absence of NADPH did not result in a new peak at 376 nm (Figure 7A,B) as observed with the wild-type protein.

CD Spectroscopy and Gel Filtration. To probe whether the loss of activity observed with the Cys^{55} mutants was the result of the enzyme's inability to catalyze chemistry due to loss of the Cys^{55} thiol, and not due to significant structural changes associated with the point mutation, CD analysis was carried out on the wild-type and mutant proteins (Figure 8A). The overlay spectra indicate that these proteins all exhibit essentially identical secondary structures. To evaluate whether the Cys^{55} mutants were compromised in their ability to oligomerize to the homododecameric structure exhibited by the wild-type enzyme (*1*), the native molecular weights of the mutants were determined by analytical size-exclusion chromatography. As can be seen in Figure 8B, the elution times for the wild-type and Cys^{55} mutants are identical, and result in K_D values corresponding to a dodecameric quaternary structure (Figure 8C) as previously reported (*1*). These data demonstrate that mutations of Cys^{55} are not accompanied by significant structural perturbations of the protein.

DISCUSSION

The enzyme QueF is an NADPH-dependent dehydrogenase in the queuosine biosynthetic pathway, where it is responsible for the four-electron reduction of the advanced intermediate $preQ_0$ to $preQ_1$, the latter of which is subsequently inserted into the relevant tRNA for the remainder of queuosine biosynthesis. The fundamental chemical conversion carried out by QueF is the direct reduction of the

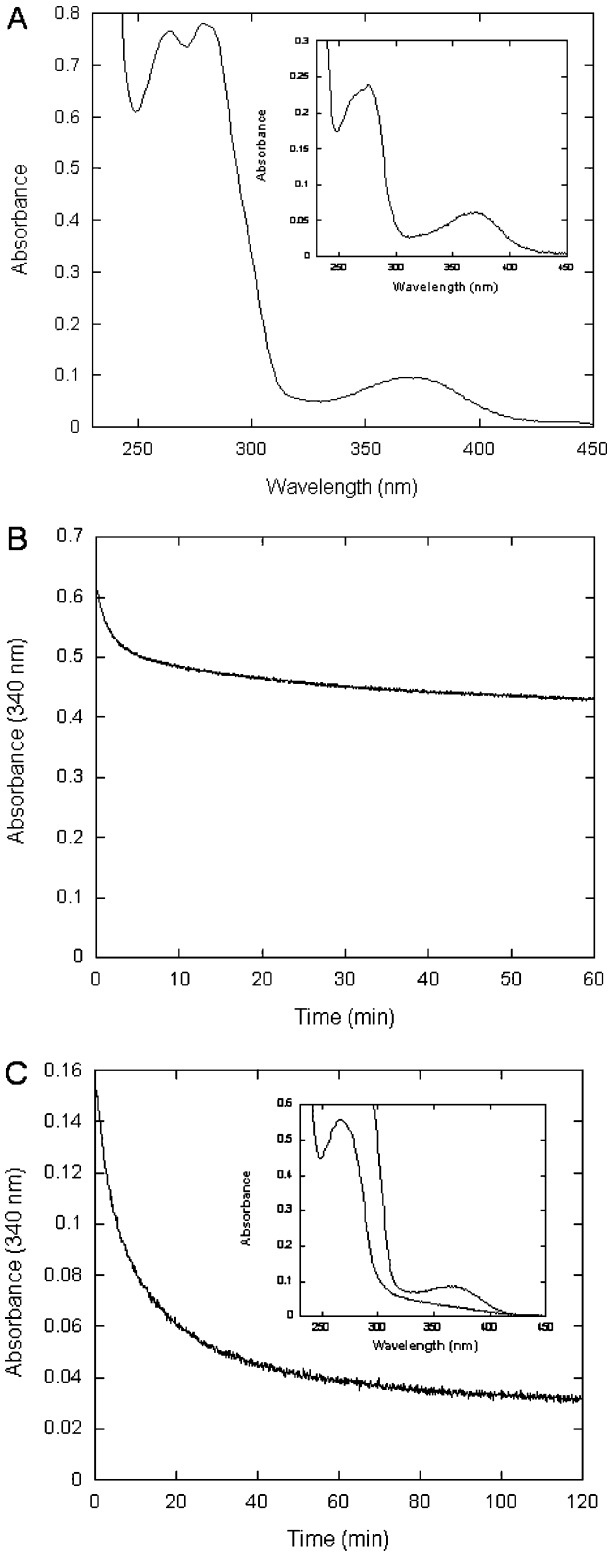

FIGURE 5: (A, main plot) UV−vis spectra of 20 μM QueF in the presence of 50 μM $preQ_0$, and after dialysis against substrate free buffer (inset). (B) Plot of the consumption of NADPH (100 μM) by the dialyzed $preQ_0$−QueF adduct. (C) Plot of the consumption of NADPH (25 μM) by the dialyzed $preQ_0$−QueF adduct (main plot), and the UV−vis spectra of the sample after the consumption of NADPH (inset, lower trace) and the addition of 50 μM $preQ_0$ (inset, upper trace).

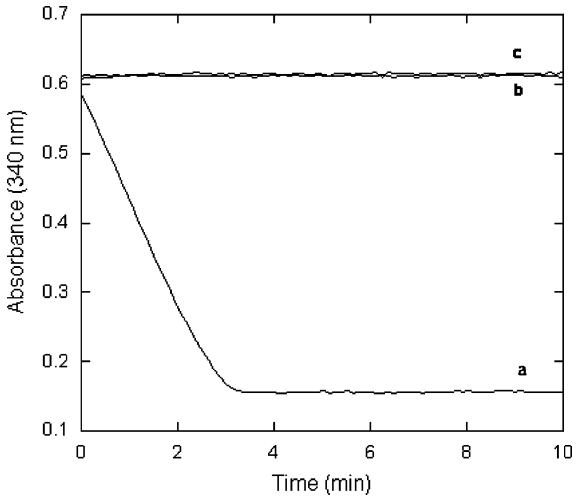

FIGURE 6: UV−vis based assay of the Cys^{55} mutants following the oxidation of NADPH. The assay solution contained 100 mM Tris (pH 7.5), 100 mM KCl, 1 mM DTT, 35 μM $preQ_0$, 100 μM NADPH, and enzyme at 30 °C. Wild-type QueF (a) at 3 μM, C55A-QueF (b) at 650 μM, C55S-QueF (c) at 270 μM. Each assay was run in triplicate, and the traces represent a single representative assay.

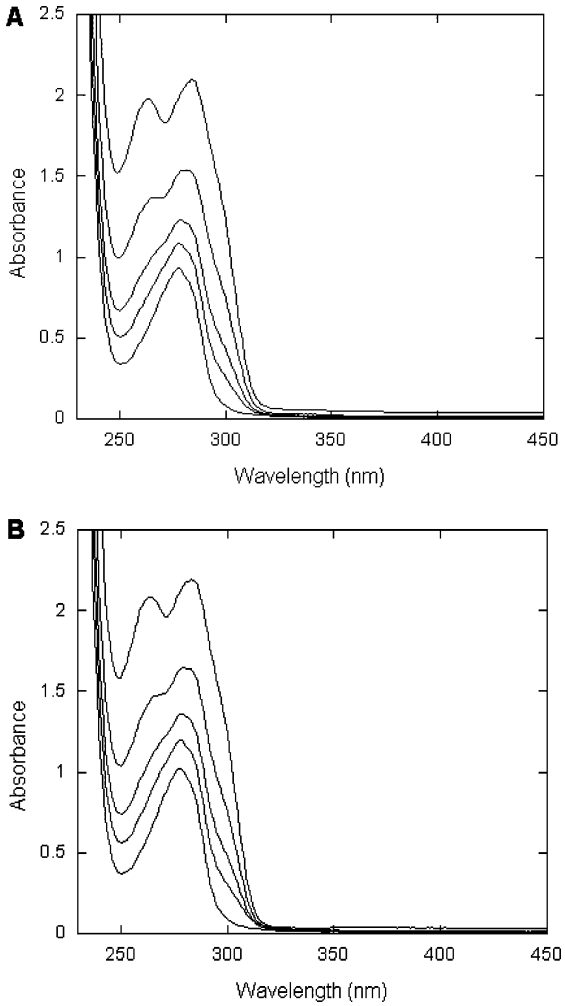

FIGURE 7: Substrate titrations of the QueF mutants C55A (A) and C55S (B). The solution contained 50 μM protein (lowest curve), followed by successive additions of $preQ_0$ to 25 μM, 50 μM, 100 μM, and 200 μM. The absorbance band at 376 nm is not observed.

nitrile functional group to that of a primary amine. With the exception of the nitrogenase catalyzed conversion of hydrogen cyanide to methylamine (*32*, *33*), the reduction of nitriles to amines has not been observed in biology. Known enzymatic transformations of nitriles include hydrolysis, giving amides or carboxylic acids as catalyzed by nitrile

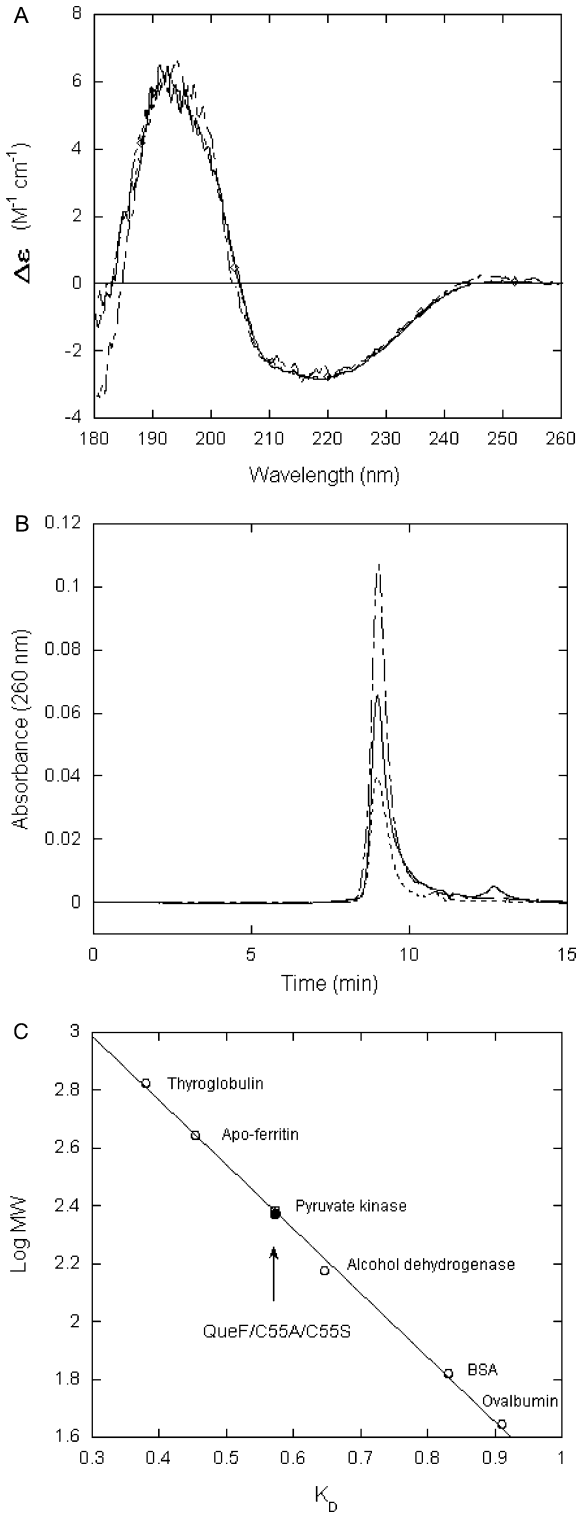

FIGURE 8: Structural investigation of wild-type and mutant QueF. (A) CD spectra of wild-type QueF (—), C55A (- — -), and C55S (— —). The enzyme concentrations were at 2 mg/mL in 20 mM phosphate buffer (pH 7.5) and 20 mM NaF. The spectra were obtained as described in Materials and Methods. (B) Size-exclusion chromatography of wild-type QueF (—), C55A QueF (- — -), and C55S QueF (— —). (C) Plot of log MW vs K_D for the protein standards thyroglobulin (670 kDa), apoferritin (443 kDa), pyruvate kinase (237 kDa), alchohol dehydrogenase (150 kDa), bovine serum albumin (66 kDa), and ovalbumin (44 kDa). K_D values were calculated according to the equation $K_D = (V_e - V_O)/(V_T - V_O)$, where V_e is the elution volume of the protein of interest, V_T = total volume, and V_O = outer volume.

hydratases and nitrilases, respectively, the oxygenase-catalyzed conversion of nitriles to cyanohydrins, and the cleavage of cyanohydrins to HCN and aldehydes or ketones by hydroxynitrile lyase.

As a prelude to more detailed kinetic analysis of the chemistry of enzyme-catalyzed nitrile reduction, steady-state kinetic analysis of QueF provided kinetic constants that are typical for the enzymes of the queuosine pathway (*30*, *31*) and NAD(P)H dependent dehydrogenases (*6*, *34*). The value of k_{cat} (0.66 min^{-1}), while on the low end of turnover numbers for dehydrogenases, is likely due to the relatively low flux through this pathway (i.e., no selective pressure to evolve highly efficient catalysis), and not a consequence of any inherent challenges posed by the reactivity of nitrile groups. Indeed, the nitrilases and nitrile hydratases exhibit k_{cat} values 10^3-10^5 fold higher (*35*−*38*) than observed here for QueF.

Sequence analysis of QueF revealed that Cys^{55} (*B. subtilis* numbering) is strictly conserved over all members in this family (*1*), and also aligns with a universally conserved Cys residue in the structurally related GTP cyclohydrolase I (GCYH I) family (*1*), where it serves as a ligand for the active-site Zn^{2+} (*19*). A homology model (*20*) of QueF predicts that, like GCYH I, the cysteine is positioned in the active site in close proximity to the substrate (*20*), and our results support this prediction; incubations of QueF with iodoacetamide, or with either Cu^{2+} or Fe^{3+}, resulted in rapid time-dependent inactivation of the enzyme, while inactivation was significantly attenuated in the presence of $preQ_0$, consistent with chemical modification (alkylation or metal-dependent oxidation) of a catalytically essential Cys residue. However, our results also clearly demonstrate that, unlike GCYH 1, QueF is not a metal-dependent enzyme, thus implicating a role in catalysis other than metal-binding for this residue.

Given the predicted proximity of Cys^{55} to the nitrile of $preQ_0$ (*20*), we reasoned that its role might be to serve as a catalytic nucleophile in the reaction, reacting with the nitrile to form a covalent thioimide intermediate which might then be the relevant species for reduction. Such an intermediate has precedence in the nitrilase-catalyzed hydrolysis of nitriles (*14*, *15*), and in a papain mutant engineered to catalyze nitrile hydrolysis (*16*). A thioimide intermediate can also be considered analogous to the thioester intermediate in the catalytic mechanism of UDP-glucose dehydrogenase (*7*), which carries out a similar nicotinamide-dependent 4-electron redox process.

Since α,β-unsaturated thioimides can possess absorptions above 350 nm (*39*), we investigated the UV−vis spectrum of the enzyme in the absence and presence of variable $preQ_0$. Titrations of substrate into enzyme resulted in the appearance of a new peak at 376 nm (Figure 4) consistent with the UV−vis absorption of an α,β-unsaturated thioimide group (*39*). The fact that this absorption reaches a maximum when substrate becomes stoichiometric with enzyme (Figure 4, inset) clearly establishes that the absorption is due to an enzyme−substrate adduct. The remarkable stability of the adduct (89% of the enzyme exists as the $preQ_0$ adduct after 3 h of dialysis), its rapid formation, and the fact that exposure to NADPH destroys the 376 nm absorbance support the proposal that the adduct is in the form of a covalent intermediate on the reaction path of QueF.

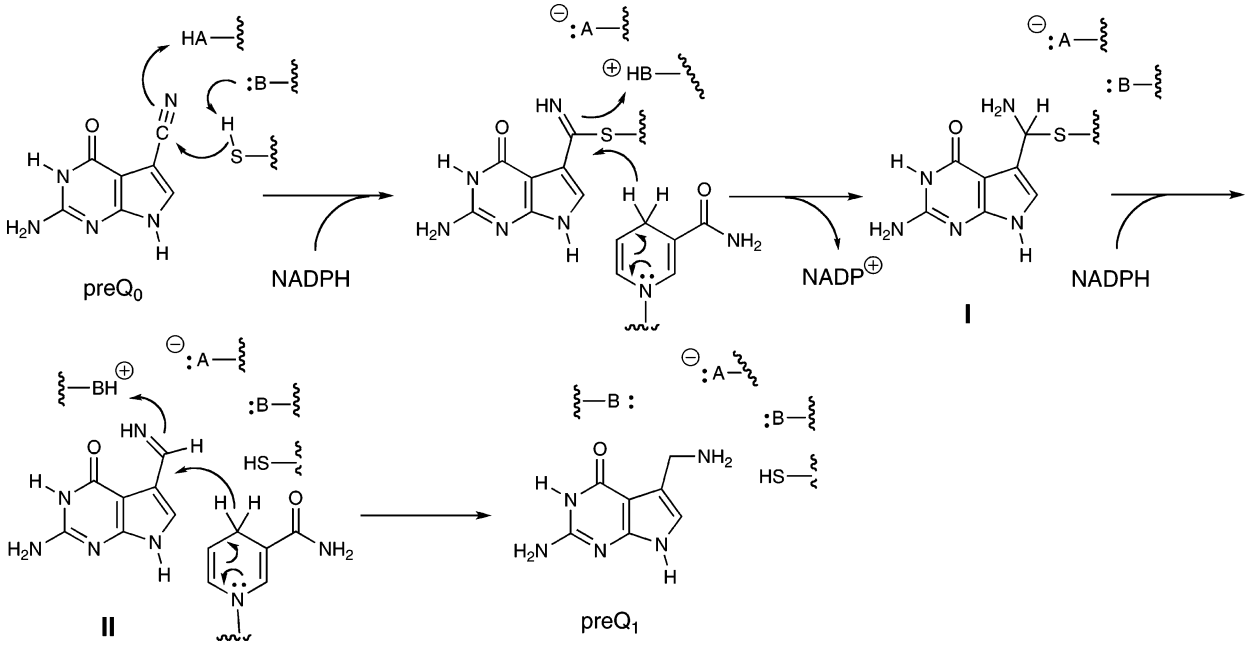

FIGURE 9: Proposed chemical mechanism for the QueF catalyzed reaction.

To further investigate the potential role of Cys^{55} in the catalytic mechanism we generated the serine and alanine point mutations of this residue (C55S and C55A). These mutations rendered the protein essentially inactive (<0.001% activity of the wild-type), and titration of the mutant proteins with $preQ_0$ resulted in no observable absorbance band at 376 nm, even at high $preQ_0$/enzyme ratios. Circular dichroism spectra of the wild-type, C55S, and C55A proteins were identical, indicating that no significant changes in secondary structure were associated with the mutations, and analytical size-exclusion chromatography demonstrated that the mutants retained the wild-type dodecamer quaternary structure. Thus, the loss of activity in the C55S and C55A mutants is consistent with the loss of essential catalytic functionality, not gross structural perturbations of the enzyme.

In contrast to the above experiments, our attempts to observe the putative covalent adduct by mass spectrometry were not successful. While the UV−vis data demonstrates that the adduct forms rapidly and is stoichiometric with enzyme concentration, the predominant species observed in the MS corresponded to the unmodified monomer unit. These results are distinct to those observed for the nitrilase-catalyzed reaction (*14*, *15*), in which a covalent adduct, although a minor species, was clearly observed in the MS spectrum. The failure to observe a covalent adduct in the QueF reaction may be due to the structure of the enzyme coupled with the instability of thioimides under aqueous conditions, especially the acidic conditions of the MS analysis (*40*). In QueF, which has a homododecamer quaternary structure (*1*), the active site is found at the interface of several subunits (*20*, *41*), and dissociation into the monomer units under the acidic conditions of the analysis exposes the adduct to hydrolytic breakdown during sample prep and/or under the ionization conditions of the MS analysis. The active site in nitrilase, on the other hand, is contained wholly within a single polypeptide (*42*), which may serve to better protect the adduct under the conditions of MS analysis.

While at this point we cannot rigorously rule out the presence of tightly bound noncovalent intermediates on the reaction path of QueF, taken together, the data support a chemical mechanism that begins with the binding of $preQ_0$ to the enzyme followed by nucleophilic attack of the thiol of Cys^{55} on the nitrile group of $preQ_0$ to form a thioimide intermediate (Figure 9). The first NADPH molecule then binds to the enzyme and reduces the thioimide intermediate, giving a new covalent adduct, the thiohemiaminal (**I**). Release of the oxidized cofactor is followed by binding of the second molecule of NADPH, collapse of the thiohemiaminal to the imine (**II**), and reduction to give $preQ_1$. Importantly, the fact that the conversion of a nitrile to an amine requires 4 electrons, and thus 2 equiv of NADPH, reveals the necessity for a covalent adduct in this enzyme catalyzed reaction; in the absence of a covalent intermediate the imine, the initial product formed from 2-electron reduction of the nitrile, would be vulnerable to hydrolysis, either in the active site itself or after dissociation from the enzyme. This is observed, for example, in the nitrogenase catalyzed reduction of HCN, where formaldehyde, the 2-electron-reduced product, and methylamine, the 4-electron-reduced product, are both significant products of the reaction (*32*, *33*). Formation of a covalent adduct in the QueF catalyzed reaction protects the intermediate imine as a thiohemiaminal after departure of the first $NADP^+$, preventing hydrolysis presumably by allowing formation of the imine only after binding of the second equivalent of NADPH.

The queuosine biosynthetic pathway has proven to be a rich source of new chemistries, and in the case of the QueF catalyzed reaction the chemistry may have useful applications beyond the realm of its role in RNA modification. There is growing interest in the use of biocatalytic transformations for industrial, synthetic, and environmental applications (*43*, *44*), and the central role of the nitrile group in these processes makes enzyme catalyzed transformations of nitriles especially relevant. For example, the nitrilase and NHase family of enzymes (*45*, *46*) have been widely implemented in industrial

biocatalytic processes (*4*, *47*). The ubiquity of nitrile reduction in industrial chemistry suggests that this area might also benefit from the introduction of a biocatalytic alternative to traditional reduction chemistries. An understanding of the mechanism of this reaction is clearly central to that goal, and we are working to elucidate additional details of nitrile reduction by this family of enzymes.

ACKNOWLEDGMENT

We thank Hans Peter Bächinger (Oregon Health and Sciences University) for the use of his CD spectrometers and his expertise, and Antonio Sarno for technical help. Finally, we thank Valérie de Crécy-Lagard (University of Florida) and Manal Swairjo (Western University of Medicine) for lively discussions on the evolution and structure−function of the QueF family of enzymes.

SUPPORTING INFORMATION AVAILABLE

pH profile of QueF activity (Figure S1), QueF activity as a function of monovalent salt (Figure S2), plot for determination of the extinction coefficient of the $preQ_0$−QueF adduct (Figure S3), and fluorescence-based activity assay plot of wild-type QueF and Cys^{55} mutants (Figure S4). This material is available free of charge via the Internet at http://pubs.acs.org.

REFERENCES

1. Van Lanen, S. G., Reader, J. S., Swairjo, M. A., de Crecy-Lagard, V., Lee, B., and Iwata-Reuyl, D. (2005) From cyclohydrolase to oxido-reductase: discovery of nitrile reductase activity in a common fold, *Proc. Natl. Acad. Sci. U.S.A. 102*, 4264−4269.
2. Okada, N., Noguchi, S., Kasai, H., Shindo-Okada, N., Ohgi, T., Goto, T., and Nishimura, S. (1979) Novel mechanism of post-transcriptional modification of tRNA. Insertion of bases of Q precursors into tRNA by a specific tRNA transglycosylase reaction, *J. Biol. Chem. 254*, 3067−3073.
3. Iwata-Reuyl, D. (2003) Biosynthesis of the 7-deazaguanosine hypermodified nucleosides of transfer RNA, *Bioorg. Chem. 31*, 24−43.
4. Banerjee, A., Sharma, R., and Banerjee, U. C. (2002) The nitrile-degrading enzymes: current status and future prospects, *Appl. Microbiol. Biotechnol. 60*, 33−44.
5. Feingold, D. S., and Franzen, J. S. (1981) Pyridine nucleotide-linked four-electron transfer dehydrogenases, *Trends Biochem. Sci. 6*, 103−105.
6. Campbell, R. E., Sala, R. F., van de Rijn, I., and Tanner, M. E. (1997) Properties and kinetic analysis of UDP-glucose dehydrogenase from group A streptococci. Irreversible inhibition by UDP-chloroacetol, *J. Biol. Chem. 272*, 3416−3422.
7. Ge, X., Campbell, R. E., van de Rijn, I., and Tanner, M. E. (1998) Covalent Adduct Formation with a Mutated Enzyme: Evidence for a Thioester Intermediate in the Reaction Catalyzed by UDP-Glucose Dehydrogenase, *J. Am. Chem. Soc. 120*, 6613−6614.
8. Barbosa, J. A., Sivaraman, J., Li, Y., Larocque, R., Matte, A., Schrag, J. D., and Cygler, M. (2002) Mechanism of action and NAD+-binding mode revealed by the crystal structure of L-histidinol dehydrogenase, *Proc. Natl. Acad. Sci. U.S.A. 99*, 1859−1864.
9. Istvan, E. S., Palnitkar, M., Buchanan, S. K., and Deisenhofer, J. (2000) Crystal structure of the catalytic portion of human HMG-CoA reductase: insights into regulation of activity and catalysis, *EMBO J. 19*, 819 - 830.
10. Tabernero, L., Bochar, D. A., Rodwell, V. W., and Stauffacher, C. V. (1999) Substrate-induced closure of the flap domain in the ternary complex structures provides insights into the mechanism of catalysis by 3-hydroxy-3-methylglutaryl-CoA reductase, *Proc. Natl. Acad. Sci. U.S.A. 96*, 7167−7171.
11. Huang, W., Jia, J., Cummings, J., Nelson, M., Schneider, G., and Lindqvist, Y. (1997) Crystal structure of nitrile hydratase reveals a novel iron centre in a novel fold, *Structure 5*, 691−699.
12. Maier-Greiner, U. H., Obermaier-Skrobranek, B. M., Estermaier, L. M., Kammerloher, W., Freund, C., Wulfing, C., Burkert, U. I., Matern, D. H., Breuer, M., Eulitz, M., and et al. (1991) Isolation and properties of a nitrile hydratase from the soil fungus Myrothecium verrucaria that is highly specific for the fertilizer cyanamide and cloning of its gene, *Proc. Natl. Acad. Sci. U.S.A. 88*, 4260−4264.
13. Payne, M. S., Wu, S., Fallon, R. D., Tudor, G., Stieglitz, B., Turner, I. M., Jr., and Nelson, M. J. (1997) A stereoselective cobalt-containing nitrile hydratase, *Biochemistry 36*, 5447−5454.
14. Stevenson, D. E., Feng, R., and Storer, A. C. (1990) Detection of covalent enzyme-substrate complexes of nitrilase by ion-spray mass spectroscopy, *FEBS Lett. 277*, 112−114.
15. Stevenson, D. E., Feng, R., Dumas, F., Groleau, D., Mihoc, A., and Storer, A. C. (1992) Mechanistic and structural studies on Rhodococcus ATCC 39484 nitrilase, *Biotechnol. Appl. Biochem. 15*, 283−302.
16. Dufour, E., Storer, A. C., and Menard, R. (1995) Engineering nitrile hydratase activity into a cysteine protease by a single mutation, *Biochemistry 34*, 16382−16388.
17. Reddy, S. Y., Kahn, K., Zheng, Y. J., and Bruice, T. C. (2002) Protein engineering of nitrile hydratase activity of papain: molecular dynamics study of a mutant and wild-type enzyme, *J. Am. Chem. Soc. 124*, 12979−12990.
18. Colloc'h, N., Poupon, A., and Mornon, J. P. (2000) Sequence and structural features of the T-fold, an original tunnelling building unit, *Proteins 39*, 142−154.
19. Auerbach, G., Herrmann, A., Bracher, A., Bader, G., Gutlich, M., Fischer, M., Neukamm, M., Garrido-Franco, M., Richardson, J., Nar, H., Huber, R., and Bacher, A. (2000) Zinc plays a key role in human and bacterial GTP cyclohydrolase I, *Proc. Natl. Acad. Sci. U.S.A. 97*, 13567−13572.
20. Swairjo, M. A., Reddy, R. R., Lee, B., Van Lanen, S. G., Brown, S., de Crécy-Lagard, V., Iwata-Reuyl, D., and Schimmel, P. (2005) Crystallization and preliminary X-ray characterization of the nitrile reductase QueF−a queuosine biosynthesis enzyme, *Acta Crystallogr. F61*, 945−948.
21. Bradford, M. (1976) A rapid and sensitive method for the quantitation of microgram quantities of protein utilizing the principle of protein-dye binding, *Anal. Biochem. 72*, 248−254.
22. Gill, S. C., and von Hippel, P. H. (1989) Calculation of protein extinction coefficients from amino acid sequence data, *Anal. Biochem. 182*, 319−326.
23. Migawa, M. T., Hinkley, J. M., Hoops, G. C., and Townsend, L. B. (1996) A Two Step Synthesis of the Nucleoside Q Precursor 2-Amino-5-cyanopyrrolo[2,3-*d*]pyrimidin-4-one ($PreQ_0$), *Synth. Commun. 26*, 3317−3322.
24. Ellis, K. J., and Morrison, J. F. (1982) Buffers of constant ionic strength for studying pH-dependent processes, *Methods Enzymol. 87*, 405−426.
25. Flamm, W. G., and Crandall, D. I. (1963) Purification of mammalian homogentisate oxidase and evidence for the existence of ferrous mercaptans in the active center, *J. Biol. Chem. 238*, 389−396.
26. Tsotsou, G. E., Cass, A. E., and Gilardi, G. (2002) High throughput assay for cytochrome P450 BM3 for screening libraries of substrates and combinatorial mutants, *Biosens. Bioelectron. 17*, 119−131.
27. Burger, E., and Gorisch, H. (1981) Patterns of product inhibition of a bifunctional dehydrogenase; L-histidinol:NAD+ oxidoreductase, *Eur. J. Biochem. 116*, 137−142.
28. Gorisch, H. (1979) Steady-state investigations of the mechanism of histidinol dehydrogenase, *Biochem. J. 181*, 153−157.
29. Grubmeyer, C. T., Chu, K. W., and Insinga, S. (1987) Kinetic mechanism of histidinol dehydrogenase: histidinol binding and exchange reactions, *Biochemistry 26*, 3369−3373.
30. Hoops, G. C., Townsend, L. B., and Garcia, G. A. (1995) tRNA-guanine transglycosylase from Escherichia coli: structure-activity studies investigating the role of the aminomethyl substituent of the heterocyclic substrate $PreQ_1$, *Biochemistry 34*, 15381−15387.
31. Van Lanen, S. G., Kinzie, S. D., Matthieu, S., Link, T., Culp, J., and Iwata-Reuyl, D. (2003) tRNA modification by S-adenosylmethionine:tRNA ribosyltransferase-isomerase. Assay development and characterization of the recombinant enzyme, *J. Biol. Chem. 278*, 10491−10499.
32. Fisher, K., Dilworth, M. J., and Newton, W. E. (2006) Azotobacter vinelandii vanadium nitrogenase: formaldehyde is a product of catalyzed HCN reduction, and excess ammonia arises directly from catalyzed azide reduction, *Biochemistry 45*, 4190−4198.

33. Hwang, J. C., and Burris, R. H. (1972) Nitrogenase-catalyzed reactions, *Biochim. Biophys. Acta 283*, 339−350.
34. Teng, H., and Grubmeyer, C. (1999) Mutagenesis of histidinol dehydrogenase reveals roles for conserved histidine residues, *Biochemistry 38*, 7363−7371.
35. Banerjee, A., Kaul, P., and Banerjee, U. C. (2006) Purification and characterization of an enantioselective arylacetonitrilase from Pseudomonas putida, *Arch. Microbiol. 184*, 407−418.
36. Kobayashi, M., Yanaka, N., Nagasawa, T., and Yamada, H. (1990) Purification and characterization of a novel nitrilase of Rhodococcus rhodochrous K22 that acts on aliphatic nitriles, *J. Bacteriol. 172*, 4807−4815.
37. Nagasawa, T., Nanba, H., Ryuno, K., Takeuchi, K., and Yamada, H. (1987) Nitrile hydratase of Pseudomonas chlororaphis B23. Purification and characterization, *Eur. J. Biochem. 162*, 691−698.
38. Nagasawa, T., Ryuno, K., and Yamada, H. (1986) Nitrile hydratase of Brevibacterium R312−purification and characterization, *Biochem. Biophys. Res. Commun. 139*, 1305−1312.
39. Hirayama, K. (1967) *Handbook of Ultraviolet and Visible Absorption Spectra of Organic Compounds*, Plenum Press Data Division, New York.
40. Neilson, D. G. (1991) Imidates including cyclic imidates, in *The chemistry of amidines and imidates* (Patai, S., and Rappoport, Z., Eds.) pp 425−483, John Wiley & Sons, New York.
41. Colloc'h, N., Mornon, J., and Camadro, J. (2002 Aug 28) Towards a new T-fold protein?: the coproporphyrinogen III oxidase sequence matches many structural features from urate oxidase, *FEBS Lett. 526*, 5−10.
42. Brenner, C. (2002) Catalysis in the nitrilase superfamily, *Curr. Opin. Struct. Biol. 12*, 775−782.
43. Schmid, A., Dordick, J. S., Hauer, B., Kiener, A., Wubbolts, M., and Witholt, B. (2001) Industrial biocatalysis today and tomorrow, *Nature 409*, 258−268.
44. Koeller, K. M., and Wong, C. H. (2001) Enzymes for chemical synthesis, *Nature 409*, 232−240.
45. Brady, D., Beeton, A., Zeevaart, J., Kgaje, C., van Rantwijk, F., and Sheldon, R. A. (2004) Characterisation of nitrilase and nitrile hydratase biocatalytic systems, *Appl. Microbiol. Biotechnol. 64*, 76−85.
46. Kobayashi, M., and Shimizu, S. (2000) Nitrile hydrolases, *Curr. Opin. Chem. Biol. 4*, 95−102.
47. Mylerova, V., and Martínková, L. (2003) Synthetic Applications of Nitrile-Converting Enzymes, *Curr. Org. Chem. 7*, 1−17.

BI701265R